Article:
Adu-Amankwah, S, Khatib, JM, Searle, DE et al. (2016) Effect of synthesis parameters on the performance of alkali-activated non-conformant EN 450 pulverised fuel ash. Construction and Building Materials, 121. pp. 453-459. ISSN: 0950-0618

https://doi.org/10.1016/j.conbuildmat.2016.05.132

Effect of synthesis parameters on the performance of alkali-activated Non-conformant EN 450 Pulverised Fuel Ash

S. Adu-Amankwah, J.M. Khatib, D.E. Searle, L.Black

Abstract

The fly ash reported in this paper is coarser than conventional pulverised fuel ash (PFA), with loss on ignition (LOI) exceeding 10.8%. Consequently, it is precluded from being used as a supplementary cementitious material (SCM) according to EN 450 and disposed in landfills. Alkali-activation of such PFAs is considered here. Three concentrations of sodium hydroxide (NaOH) were separately blended with water glass at different ratios to modify the silica modulus. Heat of reaction, setting time, compressive strength and drying shrinkage were investigated as a function of activator composition. Specimens were either cured at room temperature or hydro-thermally treated at 75°C for five hours. The results show that by optimizing the activator composition, a binder with a 28 day compressive strength of 25MPa can be synthesised from such PFAs even at room temperature. Among the activator parameters, the alkali content was observed to be most influential.

Keywords: Geopolymer, fly ash, loss on ignition, shrinkage, setting time, EN 450

1.0 Introduction

Alkali-activated binders present a low-carbon alternative to Portland cement [1]. This class of binders are obtained from the reaction between alumina-silicate feedstock and concentrated solutions of alkali hydroxides [2, 3], silicates [4], sulphates [5], carbonates [6] or combinations thereof [7, 8]. An overview of the mechanism responsible for the transformation of the initial constituent materials into a binder has been extensively reported [9, 10]. At higher pH, reactive alumina and silicates dissolve from the feedstock and when speciation equilibrium conditions are attained, the species precipitate into gels. Progressive interconnectivity of precipitated species, reorganization and condensation lead to a solid binder phase.

The parameters which influence the fresh and hardened properties of alkali-activated binders fall into two categories. That is, those inherent within the constituent materials, and the externally applied conditions. With regards to the intrinsic parameters, a variety of activators have been studied [11-14], as have a variety of feedstock materials [13-15]. The proportioning of these materials are system specific [16, 17] and consequently determine the properties of the binder produced [3]. The effect of silica moduli [4, 18, 19], silicate to alumina [20-22] and water to silicate ratios have all been explored. However, mechanical performance is usually related to the silica modulus [23, 24]. Recent studies have suggested that the amorphous silica to alumina ratio (SiO_2/Al_2O_3) also plays a significant role on the early age properties [25]. The optimum SiO_2/Al_2O_3 ratio however depends on the calcium content of the feedstock [26, 27]. It therefore follows that a generalised mix formulation in these binders does not exist, thus necessitating the need to optimize the activator composition for every feedstock.

A range of alumina-silicate source materials for the synthesis of this class of binders have been explored in the literature [28-31]. Most of the explored feedstock however requires thermal or mechanical processing in order to obtain reasonable performance [32-37]. As a result, pulverised fuel ash (PFA), an industrial by-product which can be used directly will remain a popular and rather cheaper option. By virtue of being an industrial waste, the properties of PFA are dependent on coal source [25], pulverisation and combustion conditions [38, 39] which are often tailored to maximize energy output rather than the quality of the ash. Technology and control of environmental pollution also dictates the ash collection method which also impacts on the quality of the PFA [40]. This leads to wide compositional variability, even from a single power stations [41, 42].

The variability of PFAs even from the same source restricts the use of some PFAs as SCMs. For example, the European norm EN 450-1 imposes compositional and physical requirements for PFA as SCMs; unburnt carbon content below 9%, as well as a maximum content of 40% coarser than 45 microns [43]. These non-conformant PFAs end up as landfill wastes at a cost to power generators. Previously reported alkali-activated PFAs offer potential technical advantages. However, the PFA feedstock mostly conforms to the EN 450 criteria [3, 44-48] thus competing with those used as SCMs in composite cements. The suitability of Non conformant PFA for geopolymer synthesis has not been studied previously and constitutes the objective of this paper.

2.0 Experimental Details

2.1 Materials

Unconditioned PFA obtained directly from electrostatic precipitating hubs from a UK Power station was used for this study. The X-ray fluorescence (XRF) composition and the particle size distribution obtained through Malvern Mastersizer are shown in Table 1 and Figure 1 respectively.

Table 1 XRF composition of the PFA under investigation

Oxide	SiO_2	Al_2O_3	Fe2O	CaO	MgO	Na_2O	K_2O	TiO_2	SO_2	LOI
%	51.42	24.33	13.10	4.06	2.16	0.85	2.45	1.15	0.52	10.78

Iso-propanol was used as dispersant for the PSD measurement and the Fraunhofer method was implemented for data evaluation. The LOI was separately determined according to the method in EN 196-2 hence the sum of the oxide compositions including the LOI exceeding 100%.

Activators for the study were formulated from water glass solution and laboratory grade sodium hydroxide pellets (98% purity). The water glass solution composed of 8.5±0.3 % Na_2O and 27.8±0.5% SiO_2. The viscosity and specific gravity were 70-120MPa.s and 1.385g/cm^3 respectively. Three concentrations of sodium hydroxide solutions (8, 15 and 20M) were added at different levels to modify the silica modulus

[4]. The activator composition and calculated molar ratios are shown in Table 2. The choice of the investigated activator composition range was based on the varied optimal ranges reported in the literature [49].

2.2 Sample preparation and testing

Isothermal conduction calorimetry was conducted on an 8-channel TAM Air calorimeter. 6.0g of PFA and 3.0g of the activating solutions were weighed and kept in the calorimeter until a stable baseline was attained. The activating solution was subsequently injected and then mixed in situ.

Setting time was measured on paste samples according to BS EN 196-3 using the Vicat apparatus. The entire test setup was submerged under water as prescribed in the norm. The reported setting times are average of three measurements. Mixing procedure for setting time, shrinkage and compressive strength testing were based on the recommendations of BS EN 196-1. The activating solution to feedstock ratio was maintained at 0.5. This was established from the consistency tests during the scoping studies.

Compressive strength and drying shrinkage were measured on mortar samples in replicates of three. The mortar specimens were prepared with 1:1:0.5 PFA/sand/activator ratios. The mix ratio was adopted in order to maintain the activating solution/PFA ratio at the same level as that which was used for the setting time and calorimetry measurements. The specimens for strength test were 50mm cubes. Shrinkage test was based on BS ISO 1920-8:2009 but using 40x40x160mm mortar prisms and demountable mechanical (i.e. demec) gauge studs. Measurements commenced 1 day after the relevant curing method. The demec points were attached on all four longitudinal sides of the test specimens using the polyester-based adhesive, chemical metal. Autogenous shrinkage (Auto) was taken as the shrinkage on samples sealed with flash band and monitored from 1 day. Two curing regimes were assessed; continuous curing at room temperature (RT) and hydro-thermally treated at 75°C for five hours (75), as performed elsewhere [50]. The hydro-thermal curing was achieved by introducing the moulds in a pan which was half-filled with water and covered with an aluminium foil.

Table 2 Activator composition and computed parameters

Designation	A	B	C	D	E	F	G	H	J	K	L	M	N	P	Q
NaOH conc	Group1 waterglass/8M					Group2 waterglass/15M					Group3 waterglass/20M				
SiO_2/Na_2O	0.5	1.1	1.7	2.6	3.1	0.4	0.8	1.4	2.3	3.0	0.3	0.7	1.2	2.2	2.9
Molar H_2O	5.4	5.2	5.0	4.9	7.5	4.7	4.7	4.8	4.8	7.4	4.4	4.5	4.6	4.7	6.3
H_2O/Na_2O	21	23	27	31	52	12	16	20	26	50	10	13	17	25	41

H_2O/SiO_2	39	23	16	12	17	34	20	15	12	17	31	19	14	11	14
w/solids	0.3	0.3	0.3	0.2	0.4	0.2	0.2	0.2	0.2	0.4	0.2	0.2	0.2	0.2	0.3

Note: Entries rounded to 1 decimal place.

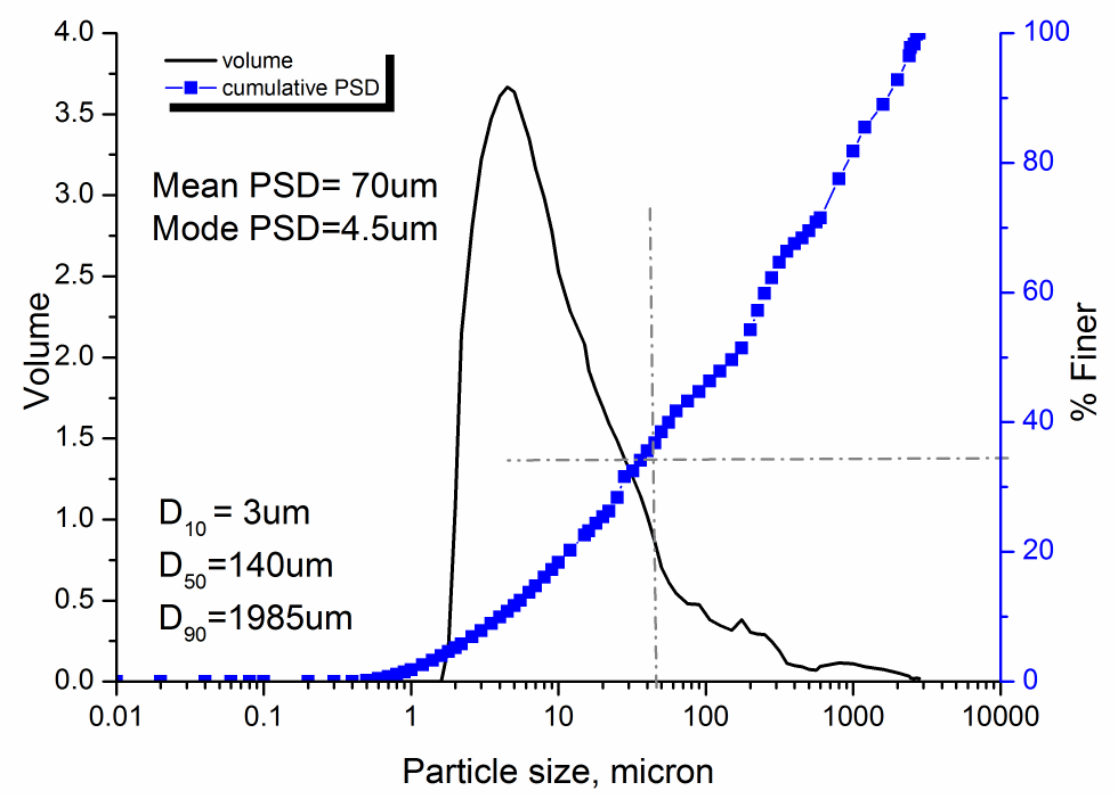

Figure 1 Particle size distribution of the PFA under investigation

3.0 Results and discussion

3.1 Reaction kinetics

The data presented here is limited to 20°C because it was not possible to perform hydrothermal curing in a calorimeter. Previous studies also converge on enhanced kinetics of reaction at elevated temperatures [3, 51, 52]. The objective here is therefore to clarify the influence of alkali concentration and dosage on the reactivity and kinetics at ambient temperature.

The kinetics of early stage reactions as a function of activator composition are shown in Figures 2 (a-c). In all formulations, the heat flow was characterized by a single exothermic peak which occurred within 20 minutes after mixing. A short induction stage can be seen in the 8M NaOH mixes (Figure 2a); but no appreciable induction was observed in the 15M and 20M mixes. The end of the induction period which was about 3 minutes in the present study marked the onset of the dissolution of silicate and aluminate species [24] from the PFA. This being distinct in the 8M NaOH activated mixes can be explained by the differences in the aluminosilicate

dissolution rate [53, 54]. The 8M NaOH activated mixes contained more water but lower hydroxyl ions compared to the 15M and 20M NaOH blends. Consequently, the increased PFA/hydroxyl ion ratio retards dissolution. This is consistent with the data from leaching experiments reported elsewhere [55].

At a given NaOH molarity, an inverse relationship was noticed between the silicate dosage and the rate of reaction. This effect was less distinct in the 8M NaOH mixes except at silica moduli of 2.6 and 3.1. Comparison between Figures 2a and 2b depicts the significance of the alkali concentration which was used to modify the silica modulus of water glass. The rate of reaction was accelerated with increasing alkali concentration. However, this seems to reach a maximum at 15M NaOH. Beyond this, differences between 15 and 20M NaOH were not visible. This may be attributed to comparable dissolution and polymerization rates at a threshold hydroxyl concentration [56]. Beyond this threshold, further increase in hydroxyl concentration has little or no influence on the overall reaction rate.

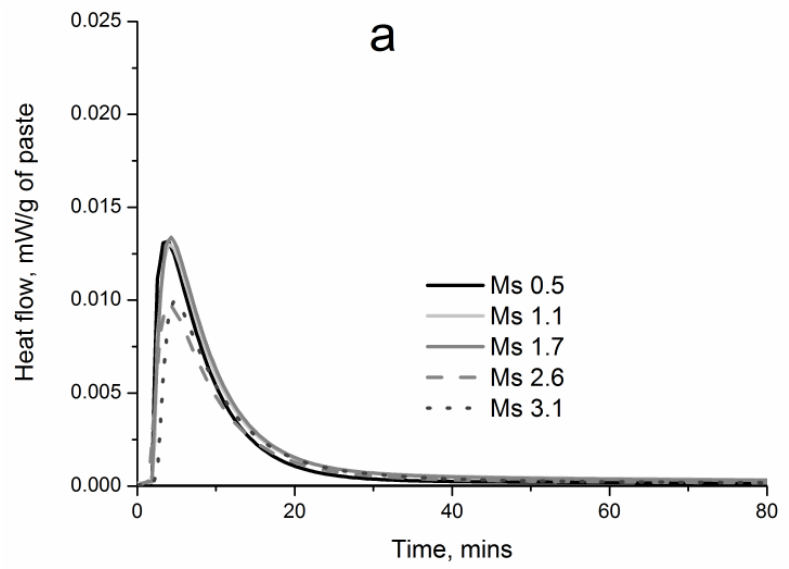

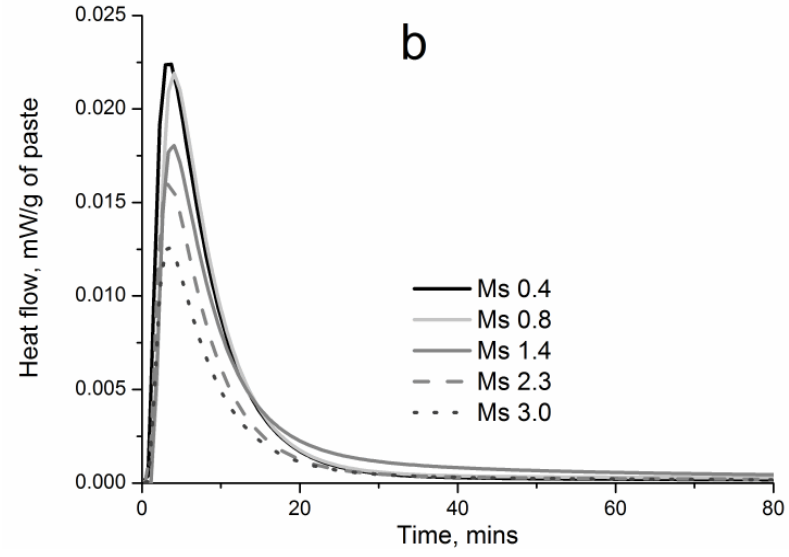

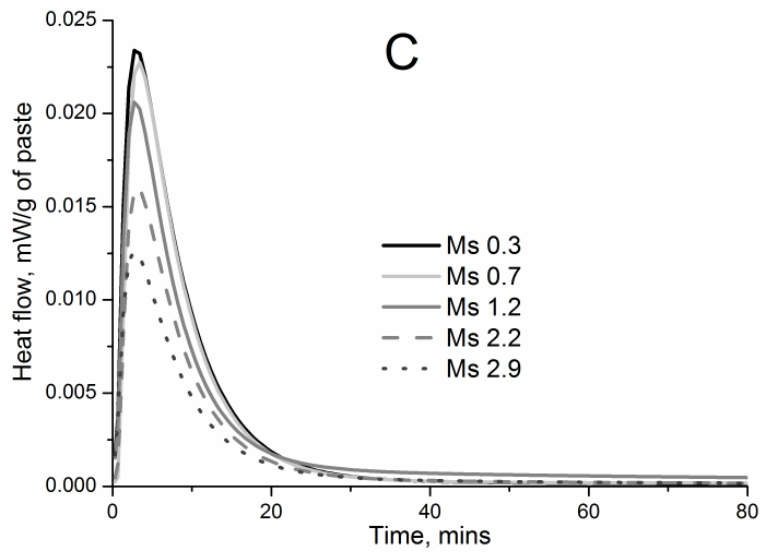

Figure 2 Effect of alkali concentration and activator composition on the heat flow of alkali-activated RoS PFA: (a) 8M NaOH blends; (b) 15M NaOH blends; (c) 20M NaOH blends. Refer to Table 2 for designations

In the synthesis of alkali-activated binders, the activator is often specified in terms of the silica moduli [24, 44, 57]. The general trend of improved rate of reaction with decreasing silica modulus is consistent with the literature [24]. However, the heat flow data presented above have shown that, slight modifications in the silica modulus can influence the reaction kinetics significantly. The mechanisms underlying these observations seem to relate to the molarity of the alkali solution rather than the silica modulus. The heat flow data is consistent with the previously espoused geopolymerisation mechanism [9, 44]. The dissolution, polymerization and condensation processes are coupled. However, dissolution is exothermic and accounts for the single heat flow peak. Subsequent reactions seem to produce minimal net heat of reaction after the first 40 minutes. Some authors [24, 56] separated the reaction rate peak into acceleration and deceleration stages which correspond to dissolution and precipitation of reaction products respectively. The maximum heat evolved for each of the three groups was plotted against the silica modulus and shown in Figure 3. This is only used as a proxy to indicate the extent of dissolution in the systems investigated and fully recognizes possible concurrent dissolution and precipitation of alumina-silicate gels [9]. The trends are similar irrespective of the alkali concentration. The maximum heat decreased with increasing silica modulus. At any given moduli, the maximum heat was similar at 15 and 20M but lower at 8M.

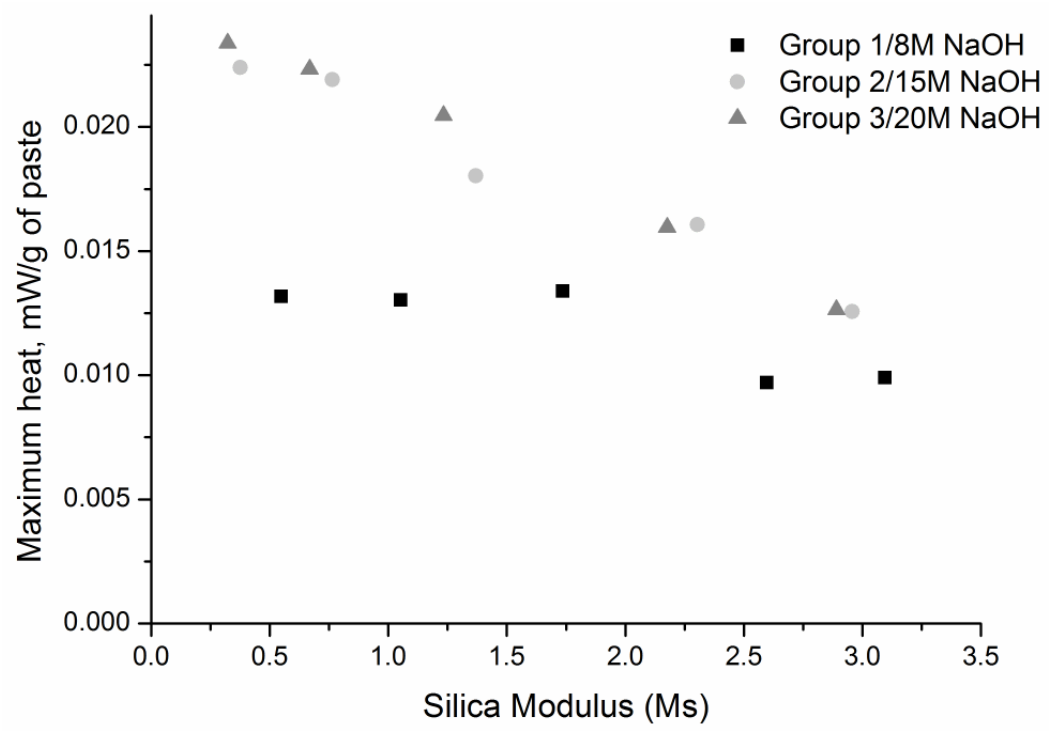

Figure 3 Effect of the silica modulus on the maximum heat evolved in activated RoS PFA

At a given molarity, increasing the dosage of the original waterglass solution reduces alkalis and the hydroxyl content. Consequently dissolution of aluminate and silicate species from the precursor is restricted. The lower evolved heat in the 8M NaOH blended binders can be explained by the suppressed dissolution and gelation at lower alkalinity [29, 55]. Recent studies reported elsewhere [58] have confirmed that persistence of aluminate species in solution inhibits further dissolution from the feedstock.

In the aqueous solution, hydrolysed silicates may be protonated and the nature may vary from monomers to oligomers [59]. The prevalence of oligomeric silicates result in gels which constitute the building blocks for the geopolymer structure. In the interlinked gels, tetrahedrally coordinated $[Al(OH)_4]]^-$ substitutes for silicates as polymerization increases. Suppressed dissolution leads to lower fraction of hydroxyl aluminates. Additionally, higher molarity increases the amount of alkalis available to balance the negative charge arising from the substitution of alumina for silicates in the evolving N-A-S-H structure [54].

3.2 Setting time

Final setting times of the investigated mixes as a function of activator composition and total w/solid ratios as measured by the Vicat method are presented in Figures 4 (a-d). Setting time, which is indicative of precipitation of network forming products, is strongly influenced by the composition of the activating solution. The strongest

correlation was observed with the silica moduli and the water to alkali ratios while the worst was observed from the water to silica ratio. According to the data, increasing the silica moduli or the water to alkali ratio of the activating solution delayed setting. The accelerating effect of higher alkali concentration on the rate of reaction and consequently quicker setting has been reported elsewhere [60]. Flash setting was observed in the mixes with SiO_2/Na_2O below one. The overall water deficiency at these moduli (SiO_2/Na_2O <1) (see Fig 2-d) potentially resulted in accelerated gelation arising from the pairing of dissolved ionic species in close proximity which then leads to rapid setting. Final setting time was over 6 hours at silica modulus of approximately 3. This may also be attributed to the lower alkali content retarding the dissolution from the feedstock [24, 55].

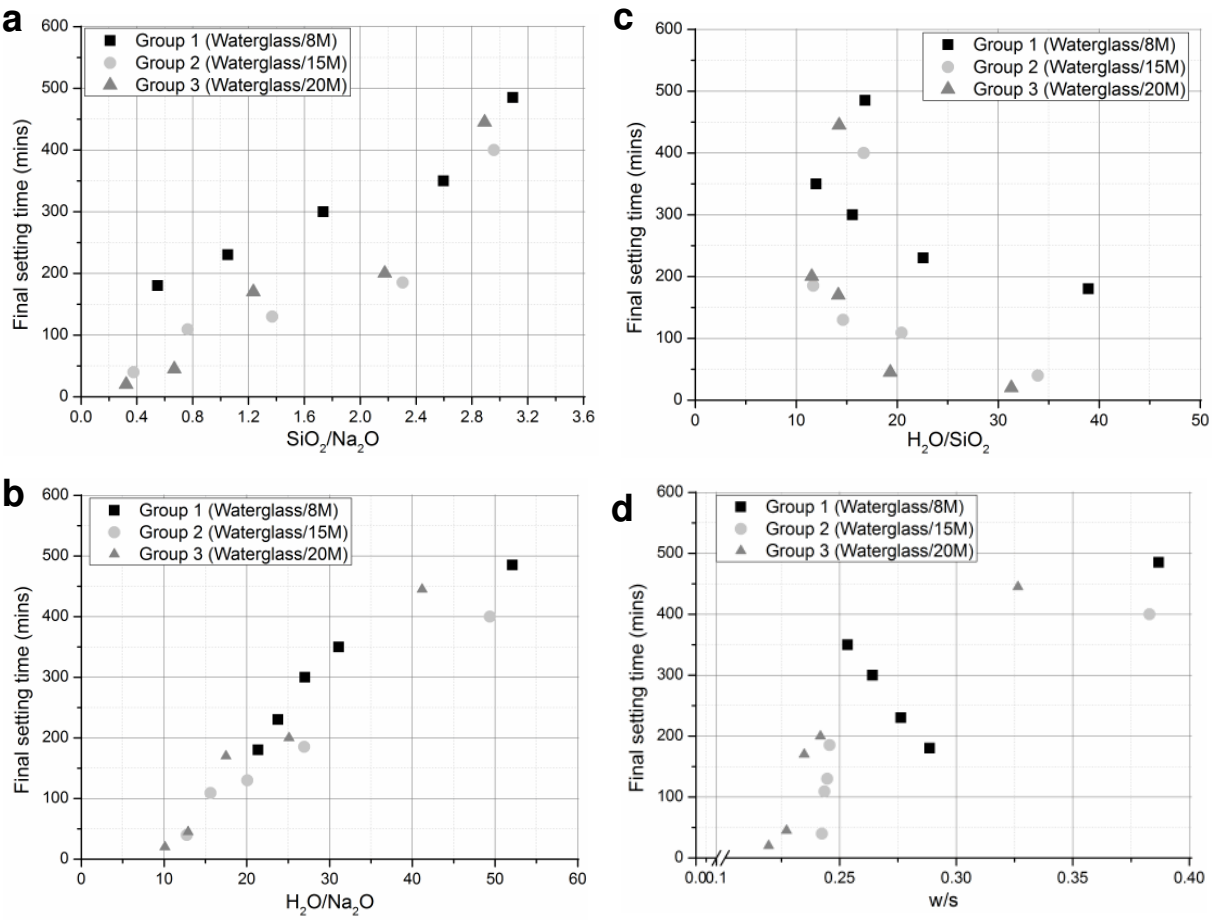

Figure 4 Initial times of RoS PFA as function of activator parameters: Effect of (a) silica modulus; (b) molar water/ alkali (c) molar water/ silica (d) water/solid ratios

Moreover, at higher silica moduli, there is the thermodynamic tendency for the silicate oligomers to polymerize at the expense of incorporating Al species [14]. This however takes place at a slower rate compared to silicate-alumina [61]. The setting times agree with the heat of reaction data presented in Figure 2 and are consistent with the trends reported in [24]. Despite the importance of alkalis to silicate dissolution, it is worth noting that excess alkalis in solution can also impede the

polymerization of the gels [62]. At SiO_2/Na_2O < 1, the Si/Al ratio of the aqueous solution is low [14] and consequently decreased alumina-silicate oligomers as already explained. Without sufficiently dissolved aluminate species, the polymeric reaction following speciation equilibrium is rather between silicates. Excess alkalinity as in the 20M NaOH blends increases the OH^- ions and eventually the water content. These hinder polymerization [63]. However, lower oligomeric alumina-silicates in the gel phase can also be beneficial for the subsequent polymerization reactions [14].

It is important to point out that the Vicat method which measures the penetration resistance of a single needle attached to a 300g plunger is not a direct measure of the evolving sodium-alumina-silicate microstructure. Despite ultrasonic measurement providing reliable assessment of the microstructural evolution [64], the Vicat test is regularly used to characterize the percolation and network formation in cementitious materials[24, 65].

3.3 Compressive strength evolution

Table 3 shows the effects of curing regime and activator composition on compressive strength after 1 and 28 days. Alongside compressive strength, the cumulative heat after 1 day is presented for each group. The impact of hydro-thermal curing on early age strength development was obvious. Compressive strength was higher following hydrothermal treatment compared to room temperature curing. The magnitude of compressive strength however depended strongly on the activator composition.

Table 3 Effects of silica modulus (Ms) and H_2O/Na_2O on compressive strength following curing at room temperature and hydrothermal curing at 75°C.

Mix ID	Ms	H_2O/Na_2O	Compressive strength, MPa @ 20°C		Compressive strength, MPa, Hydrothermal @75°C		Cum. Heat @ 1D, J/g of paste
			1D	28D	1D	28D	
A	0.54	21.37	1.43	4.80	2.91	11.67	13.48
B	1.05	23.77	5.63	14.83	16.31	23.24	15.36
C	1.74	27.02	7.10	12.59	10.82	20.33	16.60
D	2.60	31.12	3.75	5.74	4.67	6.00	9.58
E	3.09	52.10	1.35	2.55	2.10	5.72	9.75
F	0.38	12.61	1.70	11.03	3.24	12.79	19.73
G	0.76	15.62	5.90	16.24	12.99	18.68	21.24
H	1.37	20.07	11.39	25.53	19.49	35.65	32.91

J	2.30	26.94	3.79	9.59	4.26	14.92	13.52
K	2.96	49.38	1.81	2.10	1.25	3.73	10.50
L	0.32	10.11	2.65	7.17	5.84	13.11	19.01
M	0.67	12.91	4.34	14.13	6.31	15.68	23.49
N	1.23	17.49	8.12	17.30	17.10	29.10	42.98
P	2.18	25.11	4.54	13.77	4.20	14.26	12.75
Q	2.89	41.19	1.01	1.74	1.21	3.04	10.88

Note: The standard deviation the data points in the table ranged between 0.3 to 0.7MPa.

In the samples cured at room temperature, strength was lowest in the samples that were activated with 8M NaOH blended solutions. Modifying the silica modulus with 20M NaOH did not necessarily improve strength. Slightly lower strength was observed on the 20M NaOH samples which were cured at room temperature. With respect to the silica modulus, it is apparent that, irrespective of curing regime and molarity of sodium hydroxide, an optimum existed. The highest compressive strength was obtained from the moduli range 1.2 – 1.7 and water/alkali ratio of 20. The latter depends more on the alkali content than the initial water or silicate content.

These are consistent with the literature [3, 66]. This study did not reveal any distinct relationship between the H_2O/Na_2O and strength development. Plausible reason is the reaction mechanism [9] in these binders. Here, water which is consumed in the dissolution process reforms during gelation and rearrangement; silicates on the other hand only play a transitional role in the polymerization process [3, 4]. The silicates play a vital role only when dissolution of species from the feedstock is underway. The dissolved silicates in the activator then potentially act as nucleation sites for growth of polymeric chains similar to the effect of seeding on C-S-H evolution in conventional clinker based systems [67]. The nature of the resulting sodium alumina-silicate hydrate (N-A-S-H) varies according to temperature [50] and dissolved Si/Al ratios [63]among other factors.

As noticed from the heat flow data above (see Figure 2), the alkali content strongly influences the kinetics of reaction in these binders and consequently the compressive strength. A threshold alkali concentration relative to dissolved aluminates has however been reported elsewhere [60]. Silica modulus below 1.0 presents highly alkaline systems which leads to rapid super-saturation of dissolved species. This was also manifested in the setting times (Figure 4a). The excess silicates lead to coagulation of the activating solution which inhibits dissolution and subsequent polymerization.

3.4 Drying shrinkage

Figure 4 shows typical total shrinkage and shrinkage due to progressive reactions (measurement commencing after 1 day and subsequently referred to as autogenous shrinkage, denoted 'Auto') for the two curing regimes investigated; hydrothermal curing at 75ºC (denoted 75) and continuously at room temperature (denoted RT) for the PFA activated with Silica modulus of 0.8/15M. The data shows that the curing regime strongly influences total drying and autogenous shrinkage. As would be expected, water is evaporated during the hydrothermal curing. The shrinkage associated with the latter was however not taken into consideration. Following the hydrothermal curing, the sample has less water and better developed microstructure. Conversely, the room temperature cured samples reacted slowly with more water available to be removed by drying. The trend between the two curing regimes was consistent irrespective of the activator composition. This implies that, reaction persists in the room temperature cured specimens over the test duration while that of the hydrothermally cured samples were marginal. Higher drying shrinkage in the samples cured at room temperature was expected due to slower rate of reaction and availability of moisture to dissolve CO_2, thus amplifying shrinkage due to carbonation; and also evaporation of water. Carbonation related shrinkage is common in this type of binders and often manifest as efflorescence especially in ambient temperature cured samples [68]. Increasing NaOH concentration in the activator would be expected to increase shrinkage due to leaching of alkalis to form carbonates. The magnitude of this however depends on the distribution and mobility of sodium ions from the N-A-S-H gels.

The effects of activator composition on the net drying shrinkage of the investigated mixes are shown in Figure 5. The trends were similar in the hydrothermally cured samples hence not duplicated. The results show higher shrinkage with increasing silica moduli irrespective of the NaOH concentration used to modify the activating solution. The magnitude of drying shrinkage however showed strong dependence on the alkali concentration as was expected. For example, slight changes in the modulus resulting from using 15M rather than 8M NaOH doubled the drying shrinkage magnitude. However, for approximately similar modulus, the 20M NaOH showed lesser shrinkage compared to the 15M blends. In summary, highest drying shrinkage was noticed when the activator modulus was modified with 15M NaOH and lowest at the 8M NaOH. The shrinkage in the 20M NaOH blends was however higher than the 8M NaOH blends at all times. This means that shrinkage arising from leaching of alkalis is small compared to that due to moisture loss.

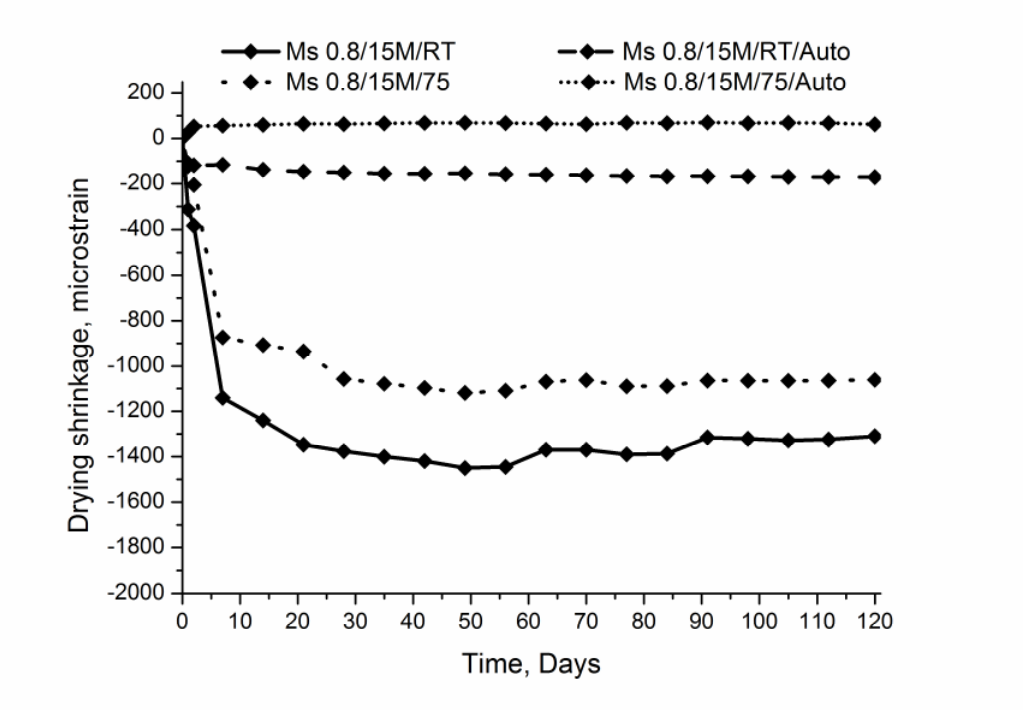

Figure 4 Effect of curing temperature on drying and autogenous shrinkage of activated RoS PFA [RT= cured at room temperature; 75ºC= hydrothermally cured at 75C; Auto= autogenous shrinkage]

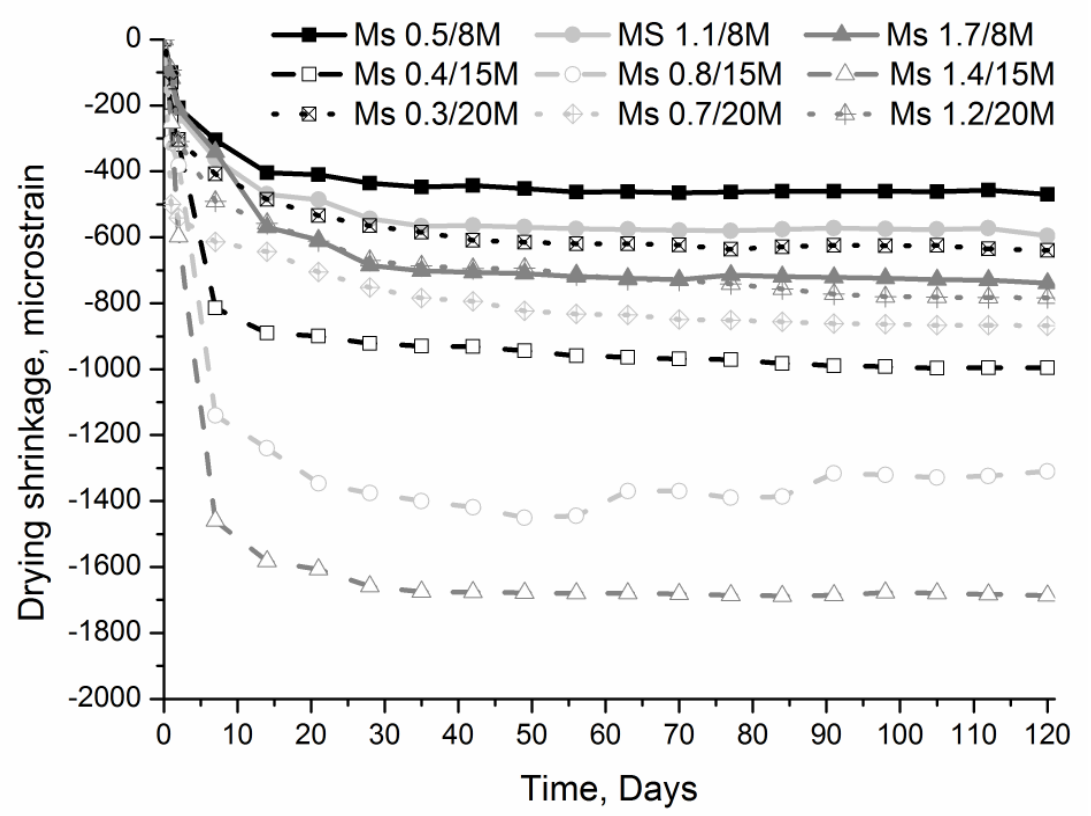

Figure 5 Effect of activator composition on the drying shrinkage of room temperature cured specimens. Solid lines: 8M NaOH; dash lines: 15M NaOH; dots= 20M NaOH blends

The observations seem to relate closely to the moisture in the specimen [69]. Considering that the water to alkali ratio increased with increasing silica modulus, higher proportion of water would be available to evaporate at high silica modulus. With regards to alkali concentration, increasing the molarity implied higher solute to water ratio as shown in Table 2; however the shrinkage did not follow this trend. The observations can be attributed to the extent of reaction in the mixes. Given that the hydrolysis of alumina-silicates consumes water but water reforms during condensation [9, 12], higher shrinkage was expected in the samples with greater reaction. This is also consistent with the compressive strength data presented above.

4.0 Conclusions

The effect of activator composition on the reaction kinetics and performance of activated high LOI PFA have been investigated. It has been shown that, by optimizing the activating solution, a binder with up to 25MPa can be produced from EN 450 non-conformant PFA at room temperature. Drying shrinkage was considerably higher than conventional cements. Regarding the activating solution parameters, the silica moduli and water/alkali ratios significantly influenced reaction kinetics, setting time, strength and dimensional stability. Reactivity improved with increasing alkali concentration but decreased at high silicate content of the activating solution. Alkali activation therefore offers the possibility of making good use PFAs which would otherwise be disposed in landfills at a cost and attendant environmental problems.

Acknowledgement

The author is thankful to the University of Wolverhampton who funded this research project.

References

[1] J.L. Provis, A. Palomo, C. Shi, Advances in understanding alkali-activated materials, Cement and Concrete Research, 78, Part A (2015) 110-125.

[2] A. Palomo, S. Alonso, A. Fernandez-Jimenez, Alkaline Activation of Fly Ashes: NMR Study of the Reaction Products, J Am Ceram Soc, 87 (2004) 1141-1145.

[3] A. Palomo, M.W. Grutzeck, M.T. Blanco, Alkali-activated fly ashes: A cement for the future, Cement and Concrete Research, 29 (1999) 1323-1329.

[4] M. Criado, A. Fernández-Jiménez, A. Palomo, I. Sobrados, J. Sanz, Effect of the SiO2/Na2O ratio on the alkali activation of fly ash. Part II: 29Si MAS-NMR Survey, Microporous and Mesoporous Materials, 109 (2008) 525-534.

[5] A.M. Rashad, Y. Bai, P.A.M. Basheer, N.C. Collier, N.B. Milestone, Chemical and mechanical stability of sodium sulfate activated slag after exposure to elevated temperature, Cement and Concrete Research, 42 (2012) 333-343.

[6] S. Bernal, J. Provis, R. Myers, R. San Nicolas, J.J. van Deventer, Role of carbonates in the chemical evolution of sodium carbonate-activated slag binders, Mater Struct, 48 (2015) 517-529.

[7] L. Verdolotti, S. Iannace, M. Lavorgna, R. Lamanna, Geopolymerization reaction to consolidate incoherent pozzolanic soil, J Mater Sci, 43 (2008) 865-873.

[8] G. Zheng, X. Cui, W. Zhang, Z. Tong, Preparation of geopolymer precursors by sol–gel method and their characterization, J Mater Sci, 44 (2009) 3991-3996.

[9] P. Duxson, A. Fernández-Jiménez, J.L. Provis, G.C. Lukey, A. Palomo, J.S.J. van Deventer, Geopolymer technology: the current state of the art, Journal of Materials Science, 42 (2007) 2917-2933.

[10] J.L. Provis, Geopolymers: Structures, Processing, Properties and Industrial Applications, in: J.S.J.v.D. J L Provis (Ed.) Geopolymers: Structures, Processing, Properties and Industrial Applications, Woodhead Publishing Materials, 2009, pp. 37-66.

[11] J. Davidovits, Geopolymers and geopolymeric materials, Journal of Thermal Analysis, 35 (1989) 429-441.

[12] A. Fernández-Jiménez, A. Palomo, M. Criado, Microstructure development of alkali-activated fly ash cement: a descriptive model, Cement and Concrete Research, 35 (2005) 1204-1209.

[13] C.K. Yip, G.C. Lukey, J.S.J. van Deventer, The coexistence of geopolymeric gel and calcium silicate hydrate at the early stage of alkaline activation, Cement and Concrete Research, 35 (2005) 1688-1697.

[14] P. Duxson, J.L. Provis, G.C. Lukey, S.W. Mallicoat, W.M. Kriven, J.S.J. van Deventer, Understanding the relationship between geopolymer composition, microstructure and mechanical properties, Colloids and Surfaces A: Physicochemical and Engineering Aspects, 269 (2005) 47-58.

[15] Z. Zhang, J.L. Provis, A. Reid, H. Wang, Mechanical, thermal insulation, thermal resistance and acoustic absorption properties of geopolymer foam concrete, Cement and Concrete Composites, 62 (2015) 97-105.

[16] Y. Chen, F. Han, L. Wu, Leaching of Lead from Geopolymer Prepared by Waste Acid Residue, Procedia Engineering, 102 (2015) 395-398.

[17] M. Izquierdo, X. Querol, J. Davidovits, D. Antenucci, H. Nugteren, C. Fernández-Pereira, Coal fly ash-slag-based geopolymers: Microstructure and metal leaching, Journal of Hazardous Materials, 166 (2009) 561-566.

[18] A.S. de Vargas, D.C.C. Dal Molin, A.C.F. Vilela, F.J.d. Silva, B. Pavão, H. Veit, The effects of Na2O/SiO2 molar ratio, curing temperature and age on compressive strength, morphology and microstructure of alkali-activated fly ash-based geopolymers, Cement and Concrete Composites, 33 (2011) 653-660.

[19] S.A. Bernal, R.M. de Gutierrez, J.L. Provis, V. Rose, Effect of silicate modulus and metakaolin incorporation on the carbonation of alkali silicate-activated slags, Cement and Concrete Research, 40 (2010) 898-907.

[20] C. Tennakoon, P.D. Silva, K. Sagoe-Crentsil, J.G. Sanjayan, Influence and role of feedstock Si and Al content in Geopolymer synthesis, Journal of Sustainable Cement-Based Materials, 4 (2015) 129-139.

[21] A. Hajimohammadi, J.L. Provis, J.S.J.v. Deventer, One-Part Geopolymer Mixes from Geothermal Silica and Sodium Aluminate, Ind Eng Chem Res, 47 (2008) 9396-9405.

[22] A. Fernández-Jiménez, A. Palomo, I. Sobrados, J. Sanz, The role played by the reactive alumina content in the alkaline activation of fly ashes, Microporous and Mesoporous Materials, 91 (2006) 111-119.

[23] A. Fernandez-Jimenez, I. García-Lodeiro, A. Palomo, Durability of alkali-activated fly ash cementitious materials, J Mater Sci, 42 (2007) 3055-3065.

[24] S.A. Bernal, J.L. Provis, V. Rose, R. Mejía de Gutierrez, Evolution of binder structure in sodium silicate-activated slag-metakaolin blends, Cement and Concrete Composites, 33 (2011) 46-54.

[25] M. Ahmaruzzaman, V.K. Gupta, Application of Coal Fly Ash in Air Quality Management, Ind Eng Chem Res, 51 (2012) 15299-15314.

[26] K. Sagoe-Crentsil, P.D. Silva, Alkali-Activated Binders: Early age nucleation reactions, chemical phase evolution and their implications on system properties, J Chin Ceram Soc, 43 (2015) 1449-1457.

[27] M. Dhakal, K. Kupwade-Patil, E.N. Allouche, C.C.L.B. Johnson, K. Ham, Optimization and Characterization of Geopolymer Mortars using Response Surface Methodology, Developments in Strategic Materials and Computational Design IV: John Wiley & Sons, Inc, (2013) 135-149.

[28] J.G.S. van Jaarsveld, J.S.J. van Deventer, G.C. Lukey, The effect of composition and temperature on the properties of fly ash- and kaolinite-based geopolymers, Chemical Engineering Journal, 89 (2002) 63-73.

[29] R.R. Lloyd, J.L. Provis, J.S.J. van Deventer, Pore solution composition and alkali diffusion in inorganic polymer cement, Cement and Concrete Research, 40 (2010) 1386-1392.

[30] G. Zheng, X. Cui, D. Huang, J. Pang, G. Mo, S. Yu, Z. Tong, Alkali-activation reactivity of chemosynthetic Al2O3–2SiO2 powders and their 27Al and 29Si magic-angle spinning nuclear magnetic resonance spectra, Particuology, 22 (2015) 151-156.

[31] K.-t. Wang, Y. He, X.-l. Song, X.-m. Cui, Effects of the metakaolin-based geopolymer on high-temperature performances of geopolymer/PVC composite materials, Applied Clay Science, 114 (2015) 586-592.

[32] C. Ruiz-Santaquiteria, A. Fernández-Jiménez, J. Skibsted, A. Palomo, Clay reactivity: Production of alkali activated cements, Applied Clay Science, 73 (2013) 11-16.

[33] C. Zhang, J. Xue, L. Fang, Mechanical perperties and microstructure of alkali-activated burned coal gangue cementitious material, J Chin Ceram Soc, 32 (2004) 1276-1280.

[34] Xinyuan Ke, Susan A. Bernal, Nan Ye, John L. Provis, J. Yang, One-Part Geopolymers Based on Thermally Treated Red Mud/NaOH Blends, J Am Ceram Soc, 98 (2015) 5-11.

[35] R.A. Antunes Boca Santa, A.M. Bernardin, H.G. Riella, N.C. Kuhnen, Geopolymer synthetized from bottom coal ash and calcined paper sludge, Journal of Cleaner Production, 57 (2013) 302-307.

[36] S. Kumar, R. Kumar, Mechanical activation of fly ash: Effect on reaction, structure and properties of resulting geopolymer, Ceramics International, 37 (2011) 533-541.

[37] J. Temuujin, R.P. Williams, A. van Riessen, Effect of mechanical activation of fly ash on the properties of geopolymer cured at ambient temperature, Journal of Materials Processing Technology, 209 (2009) 5276-5280.

[38] B. Świątkowski, E. Marek, Optimisation of pulverized coal combustion in O2/CO2/H2O modified atmosphere – Experimental and numerical study, Energy.

[39] A.J. Sarabèr, Co-combustion and its impact on fly ash quality; full-scale experiments, Fuel Processing Technology, 128 (2014) 68-82.

[40] R.S. Blissett, N.A. Rowson, A review of the multi-component utilisation of coal fly ash, Fuel, 97 (2012) 1-23.

[41] A.R. Ramsden, M. Shibaoka, Characterization and analysis of individual fly-ash particles from coal-fired power stations by a combination of optical microscopy, electron microscopy and quantitative electron microprobe analysis, Atmospheric Environment (1967), 16 (1982) 2191-2206.

[42] S. Sushil, V.S. Batra, Analysis of fly ash heavy metal content and disposal in three thermal power plants in India, Fuel, 85 (2006) 2676-2679.

[43] E. 450-1, Fly ash for concrete: Definition, specifications and conformity criteria, in, 2012.

[44] A. Fernández-Jiménez, A. Palomo, Composition and microstructure of alkali activated fly ash binder: Effect of the activator, Cement and Concrete Research, 35 (2005) 1984-1992.

[45] J.W. Phair, J.S.J. van Deventer, J.D. Smith, Effect of Al source and alkali activation on Pb and Cu immobilisation in fly-ash based “geopolymers”, Applied Geochemistry, 19 (2004) 423-434.

[46] D.L.Y. Kong, J.G. Sanjayan, K. Sagoe-Crentsil, Comparative performance of geopolymers made with metakaolin and fly ash after exposure to elevated temperatures, Cement and Concrete Research, 37 (2007) 1583-1589.

[47] K.L. Aughenbaugh, T. Williamson, M.C.G. Juenger, Critical evaluation of strength prediction methods for alkali-activated fly ash, Mater Struct, 48 (2015) 607-620.

[48] M. Komljenović, Z. Baščarević, V. Bradić, Mechanical and microstructural properties of alkali-activated fly ash geopolymers, Journal of Hazardous Materials, 181 (2010) 35-42.

[49] F. Pacheco-Torgal, J. Castro-Gomes, S. Jalali, Alkali-activated binders: A review. Part 2. About materials and binders manufacture, Construction and Building Materials, 22 (2008) 1315-1322.

[50] M. Criado, A. Palomo, A. Fernández-Jiménez, Alkali activation of fly ashes. Part 1: Effect of curing conditions on the carbonation of the reaction products, Fuel, 84 (2005) 2048-2054.

[51] J.L. Provis, J.S.J. van Deventer, Geopolymerisation kinetics. 1. In situ energy-dispersive X-ray diffractometry, Chemical Engineering Science, 62 (2007) 2309-2317.

[52] C. Shi, R.L. Day, A calorimetric study of early hydration of alkali-slag cements, Cement and Concrete Research, 25 (1995) 1333-1346.

[53] J.L. Provis, J.S.J. van Deventer, Geopolymerisation kinetics. 2. Reaction kinetic modelling, Chemical Engineering Science, 62 (2007) 2318-2329.

[54] J.L. Provis, Geopolymers and other alkali activated materials: why, how, and what?, Materials and Structures, 47 (2014) 11-25.

[55] U. Rattanasak, P. Chindaprasirt, Influence of NaOH solution on the synthesis of fly ash geopolymer, Minerals Engineering, 22 (2009) 1073-1078.

[56] S. Alonso, A. Palomo, Alkaline activation of metakaolin and calcium hydroxide mixtures: influence of temperature, activator concentration and solids ratio, Materials Letters, 47 (2001) 55-62.

[57] M. Criado, A. Fernández-Jiménez, A.G. de la Torre, M.A.G. Aranda, A. Palomo, An XRD study of the effect of the SiO2/Na2O ratio on the alkali activation of fly ash, Cement and Concrete Research, 37 (2007) 671-679.

[58] R. Snellings, Solution-Controlled Dissolution of Supplementary Cementitious Material Glasses at pH 13: The Effect of Solution Composition on Glass Dissolution Rates, J Am Ceram Soc, 96 (2013) 2467-2475.

[59] T.W. Swaddle, Silicate complexes of aluminum(III) in aqueous systems, Coordination Chemistry Reviews, 219–221 (2001) 665-686.

[60] C.A. Rees, J.L. Provis, G.C. Lukey, J.S.J. van Deventer, In Situ ATR-FTIR Study of the Early Stages of Fly Ash Geopolymer Gel Formation, Langmuir, 23 (2007) 9076-9082.

[61] P.D. Silva, K. Sagoe-Crenstil, V. Sirivivatnanon, Kinetics of geopolymerization: Role of Al2O3 and SiO2, Cement and Concrete Research, 37 (2007) 512-518.

[62] M.L. Granizo, M.T. Blanco, Alkaline activation of metakaolin – an isothermal conduction calorimetry study, J Therm Anal, 52 (1998) 957–965.

[63] C. Ruiz-Santaquiteria, J. Skibsted, A. Fernández-Jiménez, A. Palomo, Alkaline solution/binder ratio as a determining factor in the alkaline activation of aluminosilicates, Cement and Concrete Research, 42 (2012) 1242-1251.

[64] C.-W. Chung, P. Suraneni, J.S. Popovics, L.J. Struble, Setting Time Measurement Using Ultrasonic Wave Reflection, ACI Materials Journal, 109 (2012) 109-117.

[65] D.P. Bentz, C.F. Ferraris, Rheology and setting of high volume fly ash mixtures, Cement and Concrete Composites, 32 (2010) 265-270.

[66] M.S. Jansen, M.U. Christiansen, Effect of Water-solids ratio on the compressive strength and morphology of fly ash -waste glass geopolymer mortars, in: World of Coal Ash (WOCA) Conference, Nasvhille, TN, 2015.

[67] B. Mota, T. Matschei, K. Scrivener, The influence of sodium salts and gypsum on alite hydration, Cement and Concrete Research, 75 (2015) 53-65.

[68] J. Temuujin, A. van Riessen, R. Williams, Influence of calcium compounds on the mechanical properties of fly ash geopolymer pastes, Journal of Hazardous Materials, 167 (2009) 82-88.

[69] C. Kuenzel, L.J. Vandeperre, S. Donatello, A.R. Boccaccini, C. Cheesman, Ambient Temperature Drying Shrinkage and Cracking in Metakaolin-Based Geopolymers, J Am Ceram Soc, 95 (2012).